IOPscience iopscience.iop.org

Home Search Collections Journals About Contact us My IOPscience

A magnetization study of the development of short-range order in a concentrated Cu - Mn spin glass

This article has been downloaded from IOPscience. Please scroll down to see the full text article.

1996 J. Phys.: Condens. Matter 8 751

(http://iopscience.iop.org/0953-8984/8/6/016)

View the table of contents for this issue, or go to the journal homepage for more

Download details:
IP Address: 171.66.16.179
The article was downloaded on 13/05/2010 at 13:11

Please note that terms and conditions apply.

J. Phys.: Condens. Matter **8** (1996) 751–766. Printed in the UK

A magnetization study of the development of short-range order in a concentrated Cu–Mn spin glass

E MacA Gray

School of Science, Griffith University, Brisbane 4111, Australia

Received 2 August 1995, in final form 14 November 1995

Abstract. The kinetics of short-range order (SRO) growth in a **Cu**–16.4 at.% Mn alloy have been studied by measuring the evolution with time of the low-temperature magnetic properties while aging at temperatures around 100 °C. This new approach was possible because atomic SRO leads to magnetic clustering at this Mn concentration. Several models, all based on the diffusion of vacancies and their annihilation in fixed sinks, implied that the sink density was higher at 115 °C than at 100 °C for identical quenching conditions. It was concluded that the quenched-in vacancies condense in clusters. These act as sinks, halting the growth of SRO when the excess quenched-in vacancies have been absorbed. Quenching faster or aging at a higher temperature nucleates more vacancy clusters, causing earlier vacancy exhaustion. Neutron irradiation was used to continuously supply vacancies, thereby driving the SRO process to equilibrium at about 100 °C. A much higher magnetic susceptibility was attained than previously reported, some 20 times the as-quenched value at the spin freezing temperature.

1. Introduction

Copper–manganese alloys containing roughly 10–40 at.% Mn were found by Valentiner and Becker [1] to have interesting magnetic properties, manifest as a peak in the magnetization measured at low temperatures, which could be increased by aging, with maximum effect at about 22 at.% Mn. This was confirmed by Scheil and Wachtel [2], who made a comprehensive study of the effects of aging at temperatures between 100 °C and 200 °C. It was also shown that plastic deformation decreases the magnetization, and they concluded that an ordering process takes place.

Evidence for the connection between magnetic properties and short-range order (SRO) has come from many investigations using neutron scattering [3–13]. The spherically averaged atomic and magnetic SRO parameters were generally found to be negative at the nearest-neighbour (nn) position and 'in phase' among the next few neighbours, meaning that the atomic and magnetic SRO parameters tend to have the same sign, and to increase in magnitude with aging. However, a positive nn magnetic interaction was found in **Cu**–10 at.% Mn [13], along with a lower susceptibility at room temperature after aging.

The magnetic properties of these alloys have been variously described as paramagnetic, antiferromagnetic, ferromagnetic, mixtures of these and spin glassy. The 'exchange anisotropy' model of interacting ferromagnetic and antiferromagnetic domains conceived by Kouvel [14] was adapted by Beck 15] to 'micromagnetism'. In this picture the strong magnetization arises in clusters of ferromagnetically coupled spins, a position difficult to reconcile with a negative nn magnetic SRO parameter. Direct microstructural evidence for the cluster model was obtained by Gray and Smith [16], who used small-angle neutron

0953-8984/96/060751+16$19.50 © 1996 IOP Publishing Ltd

scattering to show that mesoscale entities with large magnetic moments develop at low temperatures and grow during aging at 100 °C. A later study [17] confirmed the occurrence of strong magnetic but weak nuclear scattering near $\boldsymbol{q} = \mathbf{0}$, showing that the magnetic clusters are not associated with chemical clustering [18]. These results are important pointers to the kinds of model which might be applied to experimental data on SRO kinetics.

In the light of the above, the nexus between atomic SRO and magnetic behaviour has to be regarded as empirical, on a basis yet to be elucidated.

The development of long-range order during aging has been considered many times. The spatial variation of the atomic SRO parameters in 25 at.% **Cu**–Mn [9, 12] is consistent with the development of one of the FCC superlattices [19], but the parameter magnitudes are much smaller than in the fully ordered structure. A reported observation [20] by electron microscopy of ordered precipitates in an aged 20% alloy has never been confirmed. A very recent claim for Cu_5Mn and Cu_3Mn phases [21] is contradicted by the absence of diffuse intensity at (100) and (110) required in the A_3B structure [22].

Work on understanding the growth of SRO in **Cu**–Mn during aging appeared much later than the reports devoted to defining the magnetic properties and relating them to order. The involvement of lattice defects was demonstrated by Gray and Smith [23, 24] and Tustison and Beck [25]. Pfeiler and coworkers [26–29] found that the SRO relaxation time is unreasonably long below about 200 °C, and that therefore the equilibrium degree of SRO could practically be achieved only by aging above this temperature, where the equilibrium vacancy concentration becomes sufficient to drive the ordering process. The ensuing recommendation [27] that aging should be carried out at $T = 210$–260 °C discounts the reason for so many aging studies at temperatures near 100 °C, *viz.* the much greater enhancement of the magnetic properties achievable at the lower aging temperature, despite slow kinetics [23–25], and the demonstrated decrease of SRO at high temperatures [8, 9].

Apart from in [23]–[25], little advantage has been taken of the potential of this nexus between magnetic properties and SRO for magnetic studies of SRO development. The relative changes in magnetization due to heat and mechanical treatments are much greater than those in resistivity, and the magnetization is a rather direct manifestation of the spatial extent and strength of SRO because there is no explicit contribution by vacancies to the magnetization. In this paper measurements of the kinetics of SRO growth and the ultimate degree of SRO achievable in a 16.4 at.% **Cu**–Mn alloy at relatively low aging temperatures are reported. Several models of SRO kinetics were tested against the experimental data, permitting some elucidation of the SRO mechanism.

2. Experimental details

2.1. Specimen preparation

2.1.1. Alloy manufacture The kinetic data presented here were obtained from a sample designated 3Q2, manufactured as follows. 5 N Cu and 3N8 Mn were induction melted under 1 MPa of 6 N Ar. The ingot was rolled, cut up, remelted and homogenized at 850 °C for 10 d in an evacuated quartz tube. Chemical analysis indicated a composition of 16.4 at.% Mn. The quality of the ingot was further checked by atomic absorption spectroscopy, optical microscopy and scanning electron microscope. A 3.8 mm sphere was prepared by machining and grinding.

The cylindrical magnetization samples 2Q and 2A2 were cut by spark erosion from a second ingot of nominally 16.7 at.% composition, which was prepared as above with the sole difference of arc rather than induction melting.

2.1.2. Quenching Samples 2Q and 2A2 were sealed in quartz tubes under high vacuum, held at 850 °C for about 12 h and quenched by quickly removing the capsule from the furnace and breaking it in an ice–water slurry. This conventional technique is unsatisfactory in that it is slow, virtually impossible to reproduce and relates to an unknown prequench temperature arrived at during transit between the furnace and the quenching bath [25].

Specimen 3Q2 was fast quenched from 850 °C to room temperature within a high-vacuum furnace developed by the author and P Gibbs to attain a reproducible initial state for subsequent aging experiments. The sample is dropped under vacuum into a column of silicone oil up to 1.40 m deep. An external heat exchanger on the oil column permits control of the oil temperature and thereby its viscosity, the sample velocity as it falls through the oil and the effective quench rate. A very light grinding followed to remove any surface contamination caused by reaction with the quench bath. The reproducibility of this technique was tested by quenching the same sample twice and aging it for 3 h at 100 °C. To within the resolution of the magnetization measurements, the magnetization versus temperature curve was identical from 4 to 300 K, a severe test since this aging time was sufficient to double the as-quenched peak susceptibility. Most measurements were performed after quenching with 0.43 m 20 °C oil in the column ('fast quenched'), although some were done after the sample was 'very fast quenched' into 1.40 m of 20 °C oil.

2.1.3. Aging treatments Sample 3Q2 was aged without removing it from the magnetometer. As the time taken to reach 100 °C from room temperature and vice versa was about 1 min, the shortest aging time of nominally 6 min is somewhat uncertain. The aging temperature was actively controlled to ±0.5 °C. Sample 2A2 was aged in air at 100 °C.

2.1.4. Irradiation treatment Two samples were neutron irradiated to induce a high vacancy concentration without plastic deformation. Samples 2Q and 2A2 were together exposed for 89 h to a fast-neutron flux of 3.6×10^{12} n cm^{-2} s^{-1} at an estimated in-sample temperature of 100 °C in Rig X-33 at HIFAR, the reactor of the Australian Nuclear Science and Technology Organisation. The post-irradiation sample designations were respectively 2I1 and 2I2.

2.2. Magnetic measurements

Most data were taken in a field of 9.0 Oe with a vibrating-sample magnetometer of sensitivity about 3×10^{-6} emu, carefully calibrated to permit meaningful demagnetization corrections. Measurements were possible between 1.7 and 400 K without interruption. Demagnetization corrections have been applied and all low-field data are plotted as dimensionless internal SI susceptibilities, $\chi = M$ (J T^{-1} m^{-3})$/H_{int}$ (A m^{-1}). High-field data ($H = 15$ kOe) were taken with a Foner vibrating-sample magnetometer.

3. Results

3.1. Overall aging effect and comparisons with other work

Figure 1 shows the susceptibility of sample 3Q2 after fast quenching and after aging for 96 h at 100 °C. Aging increased the susceptibility at T_f, the spin freezing temperature, to six times the as-quenched value. This factor is somewhat greater than that reported by Gibbs *et al* [30] for the same (nominal) concentration after quenching in the same apparatus and a much longer aging treatment. As the aging effect was found to increase very rapidly between 12 and 20% Mn [30], a composition difference could be responsible and T_f in

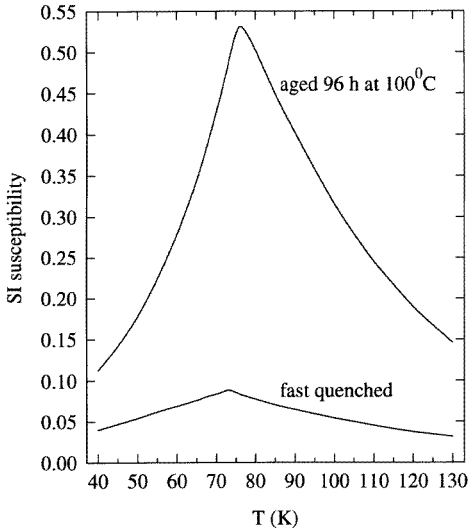

Figure 1. The low-field susceptibility of sample 3Q2 (fast quenched), as quenched and after aging for 96 h at 100 °C. $h = 9.0$ Oe.

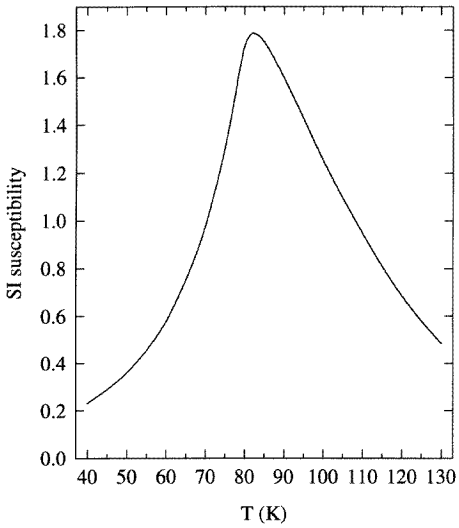

Figure 2. The low-field susceptibility of sample 2I2 (water quenched, aged 10 d at 100 °C then neutron irradiated). $H = 9.0$ Oe. Note that the peak susceptibility is 20 times that of the fast-quenched sample and that the spin freezing temperature has increased by about 9 K.

figure 1 is indeed higher than in the data shown in [30]. It should be noted that the data in [30] are too small by a factor of approximately six, due to errors in the demagnetization correction and translation from cgs to SI units.

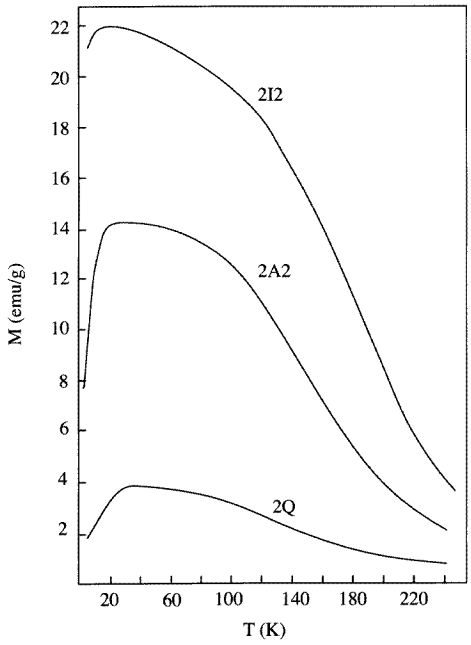

Figure 3. High-field magnetic moments of quenched, aged and irradiated samples. $H = 15$ kOe. Irradiation produced essentially the same end result in both quenched and aged samples, demonstrating that the equilibrium degree of order at the irradiation temperature has been established.

3.2. Equilibrium degree of order

Figure 2 shows the susceptibility of sample 2I2 (2A2 after irradiation). Note that the peak susceptibility has increased to *20 times* that of the fast-quenched sample (3Q2) and T_f is obviously higher. This is a much greater effect than achieved by tensile deformation of a 13% alloy [31]. In all other respects, this specimen displays the magnetic behaviour expected at this concentration. In contrast, aging specimen 3Q2 (figure 1) increased the susceptibility to less than one-third of that attained by irradiation.

Figure 3 compares the high-field magnetizations of samples 2Q (water quenched), 2A2 (aged) and 2I2. Specimen 2I1 (2Q after irradiation) had almost exactly the same magnetization as 2I2 (irradiated after aging). Hence the irradiation treatment appears to have driven the SRO process to completion at the irradiation temperature.

Figure 4 compares the effects on $\chi(T_f)$ of sample 3Q2 of aging at 100 °C and 115 °C following fast quenching, and of aging the same sample at 81 °C and 100 °C following very fast quenching. The data were extracted from magnetization versus temperature data recorded after each aging treatment. At the higher aging temperatures the susceptibility displays a clear trend to saturation far below that of the irradiated samples, even when plotted on a log time scale, a severe test for static behaviour. Either irradiation produces a state which could never be attained by aging, or the aging process is curtailed by some condition of the sample induced by its thermal history.

The maximum susceptibility reached at 115 °C is much lower than at 100 °C, confirming that the thermal history of the sample has determined the ultimate degree of SRO achievable by aging on the present, or any comparable, time scale. In common with many other systems,

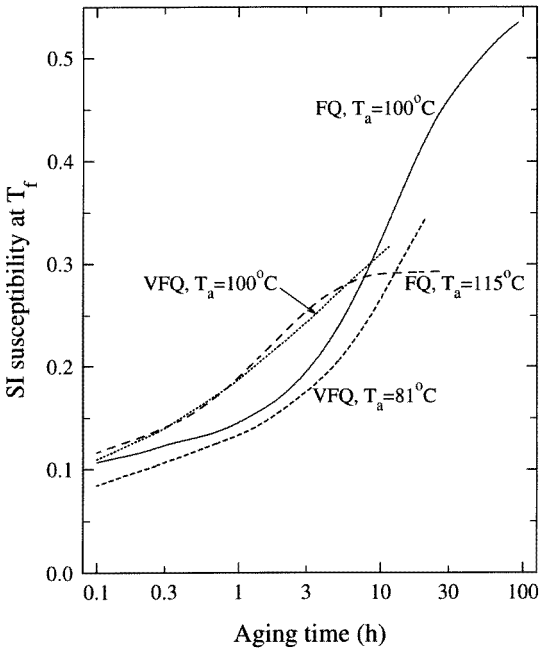

Figure 4. Aging kinetics of sample 3Q2. Solid and long-dashed lines, fast quenched and aged at 100 °C and 115 °C, respectively. Short-dashed and dotted lines, very fast quenched and aged at 81 °C and 100 °C, respectively. Note the shorter characteristic time and lower saturation susceptibility at the higher aging temperature. Note also that faster quenching has exacerbated the trend to saturation.

the vacancy concentration appears to control SRO development.

3.3. SRO kinetics

In figure 5 the kinetic behaviour of the magnetization of sample 3Q2 due to aging at 100 °C is plotted at measuring temperatures of T_f, 100, 150 and 200 K. The sigmoidal kinetic curve is characterized by a rapid rise at the same characteristic time in each case, *viz.* 2.8 ± 0.1 h. This indicates that the susceptibility truly reflects the atomic SRO, since the degree of magnetic order changes drastically in this temperature range [17].

Reconsidering figure 4 from the viewpoint of kinetics, the initial rate of SRO development is higher owing to faster quenching, indicating that a higher vacancy supersaturation was retained. However, the data taken following very fast quenching and aging at 100 °C tend towards a lower saturated value than when fast quenched. Aging at a yet lower temperature of 81 °C was required to restore an aging rate similar to that of the fast-quenched sample aged at 100 °C and lessen the tendency to early saturation.

3.4. Change in T_f during ordering

Figure 6 shows the change in T_f when specimen 3Q2 was aged at 100 °C after fast quenching. While T_f changes little relative to $\chi(T_f)$, the trend to higher temperatures is unequivocal, and linear in $\log(t)$ within the resolution of the measurement. Comparing $T_f = 76.5$ K after nearly 100 h with the value of 82 K in the irradiated sample, we can

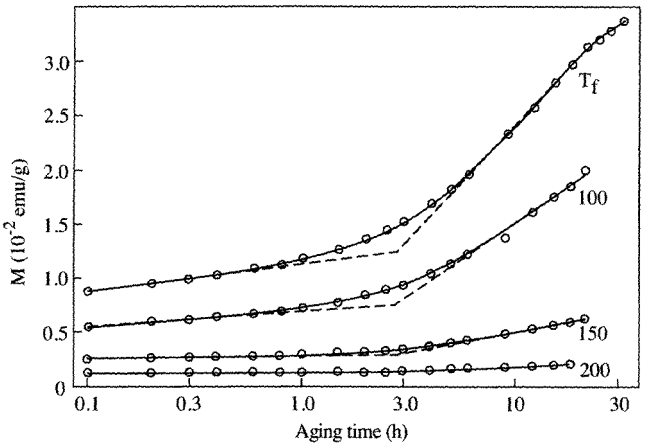

Figure 5. Aging kinetics of sample 3Q2, fast quenched, aged at 100 °C and measured at the indicated temperatures (in kelvin). The points are experimental data and the dashed lines extrapolate the solid best-fit lines to obtain the characteristic time of the ordering process. Note that this characteristic time is independent of the temperature at which it is measured.

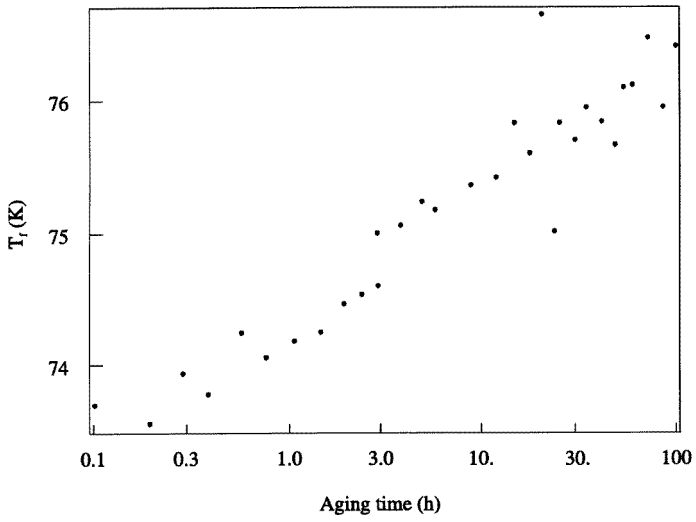

Figure 6. The increase in spin freezing temperature of sample 3Q2 when fast quenched and aged at 100 °C. Note that aging has only about one-third of the effect of irradiation.

roughly estimate that continued aging at 100 °C could require another $5\frac{1}{2}$ decades of time, or 10^9 s, to achieve the same result, in good qualitative agreement with the 2×10^9 s SRO relaxation time estimated in [27].

The ratio of the effects of aging and irradiation on T_f is about one-third, very close to the result for the peak susceptibility.

3.5. Qualitative interpretation of the results

The dependence of the ordering kinetics on quench conditions and on aging temperature, the saturation at values dependent on thermal history and the completion of ordering by irradiation all occur because the SRO process is driven by vacancy migration. Apparent saturation of the SRO occurs because the vacancy supersaturation disappears, leaving the ordering process to proceed at the rate determined by the equilibrium vacancy concentration at the aging temperature.

It is therefore clear that the effect of neutron irradiation on samples 2A2 and 2Q was to continuously create enough vacancies by well understood mechanisms (see e.g. [32]) to drive the ordering process to completion *in situ* at the temperature of the irradiation treatment. Given that the best estimate of this temperature is 100 °C, the susceptibility of specimen 2I2 reflects the equilibrium degree of SRO achievable at 100 °C.

4. Model of magnetization development due to aging

4.1. Essential model features

Two experimental phenomena must be accounted for, *viz.* the apparent saturation of the ordering process and the ubiquity of non-exponential (i.e. stretched) kinetics.

4.1.1. Non-exponential kinetics Anelasticity in general [33], and Zener relaxation in particular [34] were long ago modelled in terms of vacancy annealing. A good description of the experimental data required a distribution of vacancy relaxation times. This indicates that the origin of non-exponential SRO kinetics lies in the vacancy diffusion mechanism. In the model proposed by Schulze and Lücke [35] for SRO growth in **Au**–Ag alloys, non-exponential kinetics were accounted for by arbitrary reaction orders for both the vacancy annihilation and SRO mechanisms. While this approach gave good values for the enthalpies of vacancy formation and diffusion, it is unsupportable on physical grounds, as shown by the following considerations.

According to the diffusion model developed by Cook *et al* [36, 37], the individual Fourier components of concentration waves which develop into ordered superlattices grow with first-order kinetics, but with relaxation times depending on the spatial frequency of the concentration deviation from average. In the early stages of ordering there is amplification of many concentration spatial frequencies, but eventually the Fourier composition spectrum sharpens at positions determined by the symmetries of the reciprocal lattice [19], and a single relaxation time dominates thereafter as the superlattice appropriate to the incipient long-range order grows exponentially. Hence the SRO-induced diffuse nuclear intensities in diffraction patterns should grow exponentially and, in the present case, so should the magnetic diffuse intensity (i.e. wavevector-dependent susceptibility) and thereby the 'DC' magnetic susceptibility. The same implication is evident in the (classical, real-space) model of Dienes and Vineyard [38], in which vacancies diffuse to fixed, unfillable sinks. After an initial transient, only the zeroth-order concentration eigenfunction has appreciable amplitude, and the concentration throughout the system relaxes exponentially. According to Chik [39] however, Monte Carlo simulation of monovacancy annealing displays no initial transient. From an atomistic point of view, monovacancy migration is an activated process and should be intrinsically first order. Therefore there are several grounds on which the differential equation governing the vacancy migration should be explicitly first order.

This problem of exponential expectations but different experimental realities has been

addressed in two ways in the literature relevant to **Cu**–Mn. Kohl *et al* [40] attributed second-order aging kinetics in **Au**–Ag to the annihilation of monovacancies by association to form divacancies. Reihsner and Pfeiler [26] used the generic model of Nowick and Berry [33] to fit their non-exponential SRO kinetics. More plausible parameters (migration enthalpy etc) were obtained in this way than by fitting an exponential time dependence, but this approach is intrinsically not atomistic, so the details of the ordering mechanism cannot be disentangled. An atomistic statement of this type of model was tested against the present data, as detailed below.

4.1.2. Apparent saturation The apparent saturation of ordering well short of completion was recognised in principle [41] long before it was demonstrated in Ni–Cu [42] and in **Ni**–Cr [43]. It is readily included in model calculations by avoiding assumptions about the relative magnitudes of the quenched-in and equilibrium vacancy concentrations.

4.2. Testing against data

Four models of increasing sophistication were solved and fitted to the data, driven first by the non-exponential kinetics, then by the need to account for the dependence of aging kinetics on temperature. In all cases the mechanisms of vacancy annihilation and SRO growth are taken to be intrinsically first order. We assume that the degree of atomic SRO is described by an inverse order parameter, q, such that

$$\chi(t) = \chi_0 + (\chi_e - \chi_0)(1 - q) \tag{1}$$

where χ_0 and χ_e are respectively the initial and equilibrium susceptibilities at a given temperature (T_f in this case). χ_e is approximately known from the post-irradiation data, although never attained during the aging experiments.

The four models investigated are (i) the basic atomistic model, (ii) the monovacancy plus divacancy model, (iii) the distributed activation energy model and (iv) the vacancy cluster model.

Model (i) serves to explore the consequences of early saturation. No assumption was made about the equilibrium relative to as-quenched vacancy concentration. First-order kinetics were assumed for both vacancy annihilation in fixed sinks and SRO growth for the reasons already given. The differential equations for the vacancy concentration and order parameter are well known (see e.g. [35]) and give

$$q(t) = \exp\{-(c_e/\tau_s)[t + [(c_0 - c_e)/c_e]\tau_v(1 - e^{-t/\tau_v})]\}. \tag{2}$$

Here c_0 and c_e are the quenched-in and equilibrium vacancy concentrations. $\tau_v = n/\nu$ is the vacancy annihilation relaxation time, where a vacancy makes on average n jumps to a sink at rate ν. ν is the same as the (unconstrained) atomic jump rate because each atom jump occurs by a vacancy jump. In the limit of large n, the number of FCC lattice sites visited in n jumps is $n' = 0.744n$ [44] and $(n')^{-1} = c_s$ is just the concentration of sinks. $\tau_s = m/\nu$ is the relaxation time for SRO, where an atom makes on average ν jumps per time if there is a vacant nn site, and m is the number of jumps to reach equilibrium.

The embedded exponential in (2) changes much faster than t, so at times

$$\tau_v \ll t \ll [(c_0 - c_e)/c_e]\tau_v \tag{3}$$

the argument of the first exponential in (2) is essentially constant, and the ordering process has apparently saturated. In samples quenched from a temperature much higher than the aging temperature, $c_0 \gg c_e$, so this situation will be obtained in roughly

$$\log_{10}(c_0/c_e) = (1/\ln 10)(H_f/k_B)(1/T_a - 1/T_q) \tag{4}$$

decades of time in graphs of the form of figure 4. Taking $H_f \approx 1$ eV, $T_q = 850\,^\circ$C and $T_a = 100\,^\circ$C, apparent saturation is expected for about nine decades of time. Even allowing for an inefficient quench, and a decade or two for the inequalities in (3), saturation will occur in at least several decades of time, a convincing (but false) emulation of equilibrium. As the concentration of quenched-in vacancies or the number of vacancy jumps to annihilation decreases, the susceptibility in apparent equilibrium decreases.

The susceptibility calculated from (2) in the short-time approximation fits the experimental data poorly, as expected since the kinetics are generally non-exponential.

Schulze and Lücke [35] approximated $c_0 \gg c_e$ early in the solution of their atomistic model and the early saturation phenomenon was not predicted. Their model is readily solved exactly [43] and then exhibits early saturation. Although this model fits the experimental data presented here quite well, it involves extra parameters, is conceptually not well founded and is therefore not further considered.

In models (ii), (iii) and (iv) the exponential kinetics of model (i) are stretched in time by assuming that different physical mechanisms affect vacancy diffusion.

From the experimental observation of pure second-order aging kinetics in **Au**–Ag at high vacancy supersaturations, Kohl *et al* [40] concluded that divacancies were formed, constituting an alternative annihilation mechanism. The general case of mixed annihilation in sinks and divacancies was not solved, and so the exact solution is given here:

$$q(t) = \mathrm{e}^{-c_e t/\tau_s}\left\{\frac{1 + n\Sigma c_0[1 - (1 - c_e/c_0)\mathrm{e}^{-(1+n\Sigma c_e)t/\tau_v}]}{1 + n\Sigma c_e}\right\}^{-1/m\Sigma} \tag{5}$$

where Σ is a dimensionless effective cross section for vacancy collision [45] and all other parameters are defined as above. This model also exhibits early saturation.

A short-time approximation to (5) was fitted to the 100 °C and 115 °C aging data with much better results than from the basic atomistic model, albeit with one more fitted parameter. Table 1 summarizes the fitted parameter values. Examination of the relationships between the fitted model parameters shows that Σ must increase with T_a. Since Σ is of geometric origin [45], this is unacceptable. Hence, while fitting the data quite well, this model cannot describe their physical origin.

An alternative way to account for stretched kinetics was then evaluated, by allowing the activation energy for vacancy migration to be distributed rather than unique. We suppose that the rate equations for c and q apply to a particular ensemble of homogeneously distributed vacancies with migration enthalpy H. Assuming that this ensemble evolves independently of other ensembles with different values of H, but spatially intermingled with it, the rate equations may be solved for one ensemble, followed by the ensemble average over the distribution of migration enthalpies. Following the formalism introduced by Nowick and Berry [33],

$$\begin{aligned} \tau(H) &= \nu(H)/n = \tau_{avg}\,\mathrm{e}^{((H-H_{avg})/k_B T_a)} \\ z &= \ln\bigl(\tau/\tau_{avg}\bigr) \\ P(z) &= \bigl(1/\beta\sqrt{\pi}\bigr)\mathrm{e}^{(-z^2/\beta^2)}. \end{aligned} \tag{6}$$

Here $P(z)$ is the assumed Gaussian distribution of activation energy barriers. We assume that the annihilation efficiency n^{-1} is independent of H and ignore the possibility that a vacancy jump may take it to a site of different activation energy, i.e. one belonging to a different ensemble. The model parameters β, τ_{avg} and $c_0 n/m$ were fitted to the aging data at 100 and 115 °C by numerically performing the integral

$$\int \chi(t,\,\tau)P(z)\,\mathrm{d}z \tag{7}$$

Table 1. Parameters obtained by fitting various models of SRO growth to the aging kinetics at 100 °C and 115 °C. τ_v is the vacancy relaxation time; τ_s is the SRO relaxation time; τ_{avg} is the average relaxation time corresponding to a Gaussian distribution of energy barriers to vacancy migration; τ_n is the characteristic time for nucleation of vacancy clusters; c_0 is the quenched-in vacancy concentration; n is the number of vacancy jumps to annihilation; m is the number of atom jumps to equilibrium; Σ is the vacancy–vacancy collision cross section; β is the standard deviation of the probability distribution of energy barriers; α is the 'stretching exponent' in the JMA equation; $\gamma = 0.744\tau_n c_s(\infty)$, where $c_s(\infty)$ is the ultimate concentration of cluster sinks in the Chik model.

Aging temperature	100 °C	115 °C
Monovacancy plus divacancy model		
$n\Sigma c_0$	5.8	6.7
$\tau_v = n/\nu(h)$	32	3.5
$m\Sigma$	6.2	16
Distributed activation barrier model		
$c_0\tau_v/\tau_s = c_0 n/m$	0.33	0.13
$\tau_{avg}(h)$	17	1.6
β	1.4	1.3
Vacancy cluster nucleation and growth model (JMA)		
$c_0\tau_v/\tau_s$	0.17	0.071
$\tau_v(h)$	4.2	0.45
α	0.51	0.53
Vacancy cluster nucleation and growth model (Chik)		
$c_0\tau_n/\tau_s$ (fixed)	0.17	0.071
$\tau_n(h)$	10	1.1
γ	1.4	1.3

in place of the fitting function in a non-linear least-squares fitting program. The short-time approximation of (2) was used to obtain an expression for $\chi(t, \tau)$, preserving the intrinsic first-order kinetics. Having understood the early saturation phenomenon, it was ignored by assuming $c_e \ll c_0$. The integrator was validated by accurately reproducing the results of Nowick and Berry [33]. It is emphasized that this is conceptually quite different analysis to that applied by Reihsner and Pfeiler [26], who assumed a log-normal distribution of overall SRO relaxation times rather than vacancy relaxation times.

Table 1 lists the fitted parameters. The goodness of fit was practically indistinguishable from that of the monovacancy plus divacancy model. Examination of the fitted model parameters shows that the number of steps to annihilation for a vacancy decreases by a factor of about three between $T_a = 100$ and 115 °C, considerably more than can be due to the change in jump rate. As in model (ii), this model adequately describes the data but evidently lacks an important physical mechanism.

While the details differ, the same inference must be drawn from all the preceding modelling attempts, *viz.* that the probability of a vacancy encountering a sink is higher at 115 °C than at 100 °C. FCC metals such as Au and Cu develop secondary defects, such as vacancy clusters and loops, with a peak nucleation rate at about 0.3 T_m [46], or 100 °C in the present case. The behaviour of τ_v in the preceding models therefore implies that the quenched-in vacancies precipitate as clusters, which then act as vacancy sinks during aging. As usual in nucleation and growth, more clusters with a small average size would grow at the higher temperature. Consequently the kinetics of vacancy clustering will propagate into the kinetics of atomic SRO through the vacancy concentration.

The general problem of nucleation and growth of a precipitate phase which completely ingests a component of the parent phase is analytically intractable [47]. The present situation is even worse because the vacancy concentration appears in the SRO rate equation. Several models of the nucleation and growth of vacancy clusters have been attempted, both analytical [48, 39] and by computer simulation techniques (see e.g. [49]).

For the present purposes, an analytic expression for the concentration of nucleating sinks being necessary, the model of Chik [39] was used. The stable vacancy cluster nucleus was assumed to be a hexavacancy, formed by collisions between monovacancies, divacancies and trivacancies existing in thermal equilibrium with each other. Assuming that the capture radius of a cluster is constant, the concentration of cluster sinks was found to be [39]

$$c_s(t)/c_s(\infty) = \left(1 - \mathrm{e}^{-t/\tau_n}\right)\Big/\left(1 + \mathrm{e}^{-t/\tau_n}\right) \tag{8}$$

where τ_n is the characteristic time for cluster nucleation. The differential equation for the vacancy concentration was reconstructed, giving for the order parameter

$$-\ln q = c_0 \frac{\tau_n}{\tau_s} \int_0^{t/\tau_n} \exp\left\{-\gamma\left[u + 2\ln\left(\frac{1+\mathrm{e}^{-u}}{2}\right)\right]\right\} \mathrm{d}u \tag{9}$$

where $\gamma = 0.744\nu\tau_n c_s(\infty)$. (9) was fitted to the experimental data for the fast-quenched sample aged at 100 °C and 115 °C by performing the integral inside the least-squares fitting program as above. With the three required parameters the fit would not converge.

An alternative approach is to ignore the atomistic details of cluster nucleation and use the approximate Johnson–Mehl–Avrami equation to express the fraction of excess vacancies precipitated in clusters as

$$1 - \mathrm{e}^{-(t/\tau_v)^\alpha}. \tag{10}$$

The concentration of vacancies available to drive the SRO process, i.e. not i clusters, is then readily found, leading to a simpler integral equation for the order parameter

$$-\ln q = c_0 \frac{\tau_v}{\tau_s} \int_0^{t/\tau_v} \mathrm{e}^{-u^\alpha} \mathrm{d}u \tag{11}$$

where we have again assumed $c_e \ll c_0$ and a first-order rate equation for SRO growth.

(11) was fitted to the experimental data for the fast-quenched sample aged at 100 °C and 115 °C by performing the integral inside the least-squares fitting program as above. The values obtained for the fitted parameters are listed in table 1. The fit is shown in figure 7 (solid lines), and closely resembles those obtained from the distributed-barrier and monovacancy plus divacancy models. As expected, the characteristic time in the JMA equation, τ_v, decreases, indicating a higher rate of cluster nucleation at the higher aging temperature. The exponent α is constant within uncertainty and probably characteristic of the particular nucleation mechanism, although the value of one-half does not appear to have any particular significance. For nucleation and diffusion-controlled growth of spherical precipitates nucleated at a constant rate, the exponent in the JMA approximation is 5/2. The lower value here probably reflects the decrease in nucleation rate as the vacancy precipitation proceeds [50]. It should be remembered that the JMA equation is a 'low-impingement' approximation, which is not the case here since all excess vacancies are eventually ingested by sinks.

Since only the argument of the exponential in the integrand differs, between (9) and (11), the constant multiplying the integral should be the same in each case. Therefore the values obtained for $c_0\tau_v/\tau_s$ in the 'JMA' model were used to fix $c_0\tau_n/\tau_s$ in the Chik model, with the results shown in table 1. The fit to the data was quite poor (figure 7, dashed lines) because the exponential fall in the vacancy concentration at long times leads to an

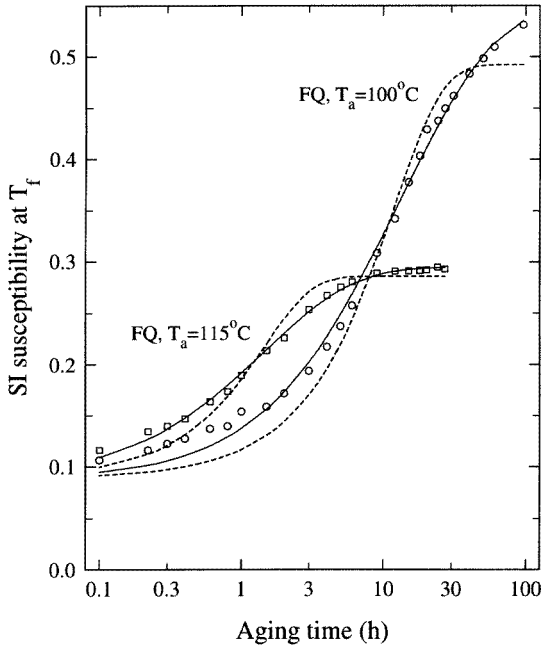

Figure 7. A comparison of the fits obtained with a model of vacancy annihilation by nucleation of vacancy clusters which then act as sinks, in the JMA approximation (solid lines) and in the nucleation model of Chik [39] (dashed lines). Points are experimental data: ○ , $T_a = 100\,^{\circ}$C; □, $T_a = 115\,^{\circ}$C. Evidently Chik's model would need to be modified by permitting a distribution of nucleation times to fit these data.

abrupt saturation like that in the basic double-first-order model. The fitted parameters are plausible, however, and confirm that the number of vacancy jumps to annihilation decreases by a factor of around three between aging temperatures of 100 °C and 115 °C. Allowing a distribution of nucleation characteristic times, τ_n, would stretch the kinetics, but as this would also make the problem intractable it is not further considered. According to Chik [39] $\tau_n \sim c_0^{-6}$, so the slightest inhomogeneity in the spatial distribution of quenched-in vacancies would have a drastic smearing effect on the kinetics.

5. Discussion

Clustering kinetics are predicted and found experimentally to be non-exponential [37, 42], i.e., they exhibit a spectrum of relaxation times and therefore tend to linear behaviour in log t. This, then, may explain the linear development of $\chi(T_f)$ in the initial stage of aging, which was not well fitted by any of the preceding models. This feature is even more apparent in results for a 17.5 at/% sample which was aged following a slower quench than achieved in the present sample [24]. The prolonged first stage of aging appears to originate in the lower concentration of quenched-in vacancies, causing a slower incubation of the 'second-phase' precipitates, i.e. vacancy clusters.

Only those models (including that of [43]) simulating rate behaviour beyond first order fitted the kinetic data reasonably well. The further choice between them relies on physical arguments. The dependence of the vacancy relaxation time on aging temperature could

not be explained except by extra vacancy sinks at the higher temperature. Therefore the cluster nucleation and growth model is the only one which can be regarded as conceptually satisfactory for rapidly quenched **Cu**–Mn alloys of the studied composition. The good fit of the generic JMA-based nucleation model relative to Chik's model suggests that distributed nucleation times contribute significantly to the aging kinetics.

Since $n \gg m$ [40], i.e. $\tau_v \gg \tau_s$, the vacancy relaxation time dominates the kinetics and characterizes the period when the SRO is changing rapidly, so a smaller value of n (the number of jumps to a sink) implies an earlier rise in SRO. Therefore we can compare experiments conducted at the same aging temperature (to fix ν) with samples prepared under different quench conditions. Comparing specimen 3Q2 when fast quenched and very fast quenched with the (relatively slowly and from a lower temperature) quenched wire specimen previously reported in [24], all aged at 100 °C, there is a strong and consistent trend toward lower n values as the quench speed increases. Quenching faster increases the initial vacancy concentration, c_0. At a fixed aging temperature the final cluster concentration must increase with the availability of more nucleation sites, i.e. at higher values of c_0. Hence more sinks are nucleated after a faster quench and n decreases as observed. n also determines the saturation value of SRO, explaining the trend in figure 4 to flatter-looking aging curves after faster quenching and aging at higher temperatures.

The much higher sink concentration apparent during aging at 115 °C compared to 100 °C suggests that most vacancy clusters are nucleated during aging, at least at these relatively high quench rates.

Further progress in modelling SRO development is likely to require outright computer experiments using Monte Carlo simulation or molecular dynamics to deal with the complexities of the interaction of vacancies with their environment. This can be seen in two aspects of the problem which are intractable to analytical techniques. (i) SRO development does not proceed in adventitious fashion, by an atom randomly arriving at a site and staying if it increases the SRO. Correlated atom movements are required [51], so the random-walk assumption implicit in this and other studies is unphysical. (ii) The changing atomic environment caused by SRO, and the distorted lattice around sinks, both modify the interatomic potentials, causing distributed activation barriers for vacancy migration and stretched kinetics. Spatial inhomogeneities in the initial distribution of vacancies will have a similar effect via the cluster nucleation time, and are unavoidable owing to inhomogeneous cooling of the sample during the quench.

The efficacy of neutron irradiation in driving the ordering process suggests that an ordered phase may grow at lower temperatures. Irradiation-induced aging at room temperature is feasible, although probably not below, because interstitials in **Cu**–Mn appear to be immobile [52]. Gibbs *et al* [30] found that the effect of aging at 100 °C peaked sharply at 20% Mn. Since the samples were quenched by the same reproducible technique used for this work, this result probably indicates incipient order of the Ni_4Mo type.

6. Conclusions

In **Cu**–16.4 at.% Mn SRO develops by vacancy migration to sinks. Because (i) the peak nucleation rate for vacancy clusters is expected to occur around the aging temperatures in this study and (ii) the probability of encountering a sink increased dramatically between 100 °C and 115 °C in all the models which had a sink density parameter, a large proportion of the vacancy sinks must be vacancy clusters or other secondary defects nucleated during aging. Some smearing of the aging kinetics by distributed cluster nucleation times probably occurs owing to an inhomogeneous distribution of quenched-in vacancies.

The saturation of the ordering process at different levels of completion owing to different quench and aging conditions demonstrates that vacancy exhaustion has occurred. The effect is exacerbated by faster quenching because more sinks are nucleated from the greater initial vacancy population.

Neutron irradiation at about 100 °C supplied sufficient vacancies to establish the equilibrium degree of SRO within the irradiation time of 89 h, in both quenched and previously aged samples. The susceptibility of the quenched sample was thereby increased 20 times, a much greater effect than previously reported by any other treatment. The possible existence of ordered phases such as Cu_4Mn should be investigated by this means.

Acknowledgments

Access to neutron irradiation facilities was provided by the Australian Institute of Nuclear Science and Engineering. Helpful discussions with T J Hicks are gratefully acknowledged.

References

[1] Valentiner S and Becker G 1933 *Z. Phys.* **80** 735
[2] Scheil E and Wachtel E 1957 *Z. Metallk.* **48** 571
[3] Meneghetti D and Sidhu S S 1957 *Phys. Rev.* **105** 130
[4] Arrott A 1965 *J. Appl. Phys.* **36** 1093
[5] Bacon G E and Cowlam N 1967 *J. Phys. C: Solid State Phys.* **2** 675
[6] Wells P and Smith J H 1971 *J. Phys. F: Met. Phys.* **1** 763
[7] Werner S A, Sato H and Yessik M 1972 *Proc. 17th Ann. Conf. on Magnetism and Magnetic Materials* ed C D Graham and J J Rhyne (New York: American Institute of Physics) p 508
[8] Werner S A, Sato H and Yessik M 1973 *Proc. 18th Ann. Conf. on Magnetism and Magnetic Materials* ed C D Graham and J J Rhyne (New York: American Institute of Physics) p 679
[9] Hirabayashi M, Koiwa M, Yamaguchi S and Kamata K 1978 *J. Phys. Soc. Japan* **45** 1591
[10] Davis J R, Surke S K and Rainford B D 1980 *J. Magn. Magn. Mater.* **15–18** 151
[11] Harders T M, Hicks T J and Smith J H 1983 *J. Phys. F: Met. Phys.* **13** 1262
[12] Cable J W, Werner S A, Felcher G P and Wakabayashi N 1984 *Phys. Rev.* B **29** 1268
[13] Ahmed N and Hicks T J 1975 *J. Phys. F: Met. Phys.* **5** 2168
[14] Kouvel J S 1961 *J. Phys. Chem. Solids* **21** 57
[15] Beck P A 1971 *Metall. Trans.* **2** 2015
[16] Gray E M and Smith J H 1975 *J. Phys. F: Met. Phys.* **5** L171
[17] Gray E M, Hicks T J and Smith J H 1982 *J. Phys. F: Met. Phys.* **12** L189
[18] Ling M F, Staunton J B and Johnson D D 1994 *J. Phys.: Condens. Matter* **6** 6001
[19] de Fontaine D 1975 *Acta Metall.* **23** 560
[20] Warlimont H, Bernecker K and Lück R 1971 *Z. Metallk.* **62** 816
[21] Gödecke T 1990 *Z. Metallk.* **81** 826
[22] Bouchiat H, Dartyge E, Monod P and Lambert M 1981 *Phys. Rev.* B **23** 1375
[23] Gray E M and Smith J H 1976 *Phys. Status Solidi* a **33** K43
[24] Gray E M and Smith J H 1977 *Solid State Commun.* **24** 143
[25] Tustison R W and Beck P A 1977 *Solid State Commun.* **21** 517
[26] Reihsner R and Pfeiler W 1985 *J. Phys. Chem. Solids* **46** 1431
[27] Pfeiler W and Reihsner R 1985 *J. Phys. F: Met. Phys.* **15** 2547
[28] Pfeiler W and Reihsner R 1986 *Phys. Status Solidi* a **97** 377
[29] Clad R, Keuntzler R and Pfeiler W 1990 *J. Phys.: Condens. Matter* **2** 6593
[30] Gibbs P, Harders T M and Smith J H 1985 *J. Phys. F: Met. Phys.* **15** 213
[31] Kahl S, Neuhaus R, Pinkvos H and Schwink C 1990 *Phys. Status Solidi* a **120** 221
[32] Johnson R A and Orlov A N (ed) 1986 *Physics of Radiation Effects in Crystals* (Amsterdam: North-Holland)
[33] Nowick A S and Berry B S 1961 *IBM J. Res. Dev.* **5** 297, 312
[34] Berry B S and Orehotsky J L 1968 *Acta Metall.* **16** 683, 697
[35] Schulze A and Lücke K 1972 *Acta Metall.* **20** 529
[36] Cook H E, de Fontaine D and Hilliard J E 1969 *Acta Metall.* **17** 765

[37] Cook H E 1969 *J. Phys. Chem. Solids* **30** 2427
[38] Dienes G J and Vineyard G H 1975 *Radiation Effects in Solids* (London: Interscience) ch 5
[39] Chik K P 1970 *Vacancies and Interstitials in Metals* ed A Seeger *et al* (Amsterdam: North-Holland) p 183
[40] Kohl W, Schefel R, Heisediek H and Lücke K 1983 *Acta Metall.* **31** 1895
[41] Lomer W M 1957 *Vacancies and Other Point Defects in Metals and Alloys* (London: Institute of Metals)
[42] Poerschke R, Theis U and Wollenberger H 1980 *J. Phys. F: Met. Phys.* **10** 67
[43] Heisediek H, Lücke K and Scheffel R 1982 *J. Phys. Chem. Solids* **43** 825
[44] Vineyard G H 1963 *J. Math. Phys.* **4** 1191
[45] Waite T R 1957 *Phys. Rev.* **107** 463
[46] Eyre B L 1973 *J. Phys. F: Met. Phys.* **3** 422
[47] Martin J W and Doherty R D 1976 *Stability of Microstructure in Metallic Systems* (Cambridge: Cambridge University Press) ch 2
[48] de Jong M and Koehler J S 1963 *Phys. Rev.* **129** 49
[49] Takamura J, Shirai Y, Furukawa K and Nakamura F 1987 *Mater. Sci. Forum* **15–18** 809
[50] Burke J 1965 *The Kinetics of Phase Transformations in Metals* (Oxford: Pergamon) ch 7
[51] Yu G and Lücke K 1992 *Acta Metall. Mater.* **40** 2523
[52] Pfeiler W and Poerschke R 1987 *J. Phys. F: Met. Phys.* **17** 1043